Noncollinear and noncoplanar magnetic order in the extended Hubbard model on anisotropic triangular lattice

Kanika Pasrija and Sanjeev Kumar
Indian Institute of Science Education and Research (IISER) Mohali, Sector 81, SAS Nagar, Manauli PO 140 306, India
(Received 21 October 2015; revised manuscript received 27 March 2016; published 6 May 2016)

Motivated by the importance of noncollinear and noncoplanar magnetic phases in determining various electrical properties in magnets, we investigate the magnetic phase diagram of the extended Hubbard model on an anisotropic triangular lattice. We map out the ground-state phase diagram within a mean-field scheme that treats collinear, noncollinear, and noncoplanar phases on equal footing. In addition to the standard ferromagnet and 120° antiferromagnet states, we find the four-sublattice flux, the 3Q noncoplanar, and the noncollinear charge-ordered states to be stable at specific values of filling fraction n. Inclusion of a nearest-neighbor Coulomb repulsion leads to intriguing spin-charge-ordered phases. The most notable of these are the collinear and noncollinear magnetic states at $n = 2/3$, which occur together with a pinball-liquid-like charge order. Our results demonstrate that the elementary single-orbital extended Hubbard model on a triangular lattice hosts unconventional spin-charge ordered phases, which are similar to those reported in more complex and material-specific electronic Hamiltonians.

DOI: 10.1103/PhysRevB.93.195110

I. INTRODUCTION

The transition metals and their oxides are well known for exhibiting a variety of magnetic ordering phenomena [1,2]. The nature of the low-temperature magnetically ordered states depends on the type of dominant magnetic exchange interactions, which in turn depend on the details of the crystal structure and electronic band structure. The theoretical models that describe the magnetism of transition metals and their oxides can be divided into three broad categories: (i) models that do not *a priori* contain a local moment but allow for moment formation via electron-electron interactions, such as the Hubbard model [3]; (ii) models consisting of localized spins only, such as the Heisenberg model; and (iii) models that have itinerant electrons coupled to localized moments, e.g., the Kondo lattice model [4]. Starting with a general multiorbital Hubbard model, the other two types can be obtained in appropriate limits [5]. Hence, the Hubbard model is the elementary model for describing magnetism. Indeed, two of the most common magnetically ordered ground states, the ferromagnet and the staggered antiferromagnet, are present in the mean-field phase diagram of the Hubbard model [6].

The search for noncollinear and noncoplanar magnetic ordering in models and materials has emerged as an important research topic in recent years. The reason is the fundamental connection between the nature of magnetic order and electrical properties of various magnetic materials. A noncoplanar magnetic order is known to give rise to anomalous Hall response in transport [7–9]. On the other hand, a planar spiral order can allow for a ferroelectric response via the spin-current mechanism [10,11]. Recent theoretical studies on Kondo-lattice models have shown that a variety of unconventional magnetic ground states can be stabilized depending on the underlying lattice geometry and electronic filling fraction. In particular, triangular and checkerboard lattices allow for noncoplanar magnetism at quarter filling of the band [12–18]. More recently, the existence of spin-charge ordered phases has also been reported at the average filling fraction of two electrons per three sites [19]. Given that the Hubbard model is the fundamental model for magnetism, it is important to know if the unconventional magnetic phases found in the Kondo-lattice Hamiltonian are also present in the Hubbard model. Moreover, for some of the magnetic phases the shape of the Fermi surface plays a crucial role and the ordered phases should therefore be independent of the nature of the interactions [12,20]. To the best of our knowledge a systematic search across the electronic density range for noncollinear and noncoplanar magnetic phases in the Hubbard model on a triangular lattice has not been reported.

In this work, we map out the magnetic phase diagram of the Hubbard model on an anisotropic triangular lattice within a variational mean-field approach that captures the noncollinear and noncoplanar magnetism on the same footing as the collinear magnetism. The phase diagram is rich and consists of many unconventional phases that are found in the corresponding Kondo-lattice model. These include (i) the four-sublattice 3Q order at quarter filling, (ii) the flux state at quarter filling, and (iii) the noncollinear charge-ordered phase at two-thirds filling. In addition, the 120° state is stable near the isotropic triangular limit and a collinear stripe state is stable in the anisotropic regime. The influence of nearest-neighbor Coulomb repulsion on these phases is also investigated. We find that a pinball-liquid-like charge-ordering phase, which has so far been reported in spinless fermion models or multiorbital models on a triangular lattice, is stabilized by the Coulomb interactions at a filling fraction of $n = 2/3$ and occurs concomitantly with either collinear or noncollinear magnetic order. Given the fundamental nature of the Hubbard Hamiltonian, our results are of general interest. In addition, the reported phases are of specific relevance to various triangular lattice systems, such as the layered $AgNiO_2$ [21,22], the $NaCoO_2$ [23–27], and the organic charge-transfer salts [28,29].

The remainder of the paper is organized as follows. In Sec. II we describe the model and briefly discuss the previous investigations that focus on noncollinear magnetism. In Sec. III we describe the method used in this work. Results and discussions follow in Sec. IV, where we first discuss the

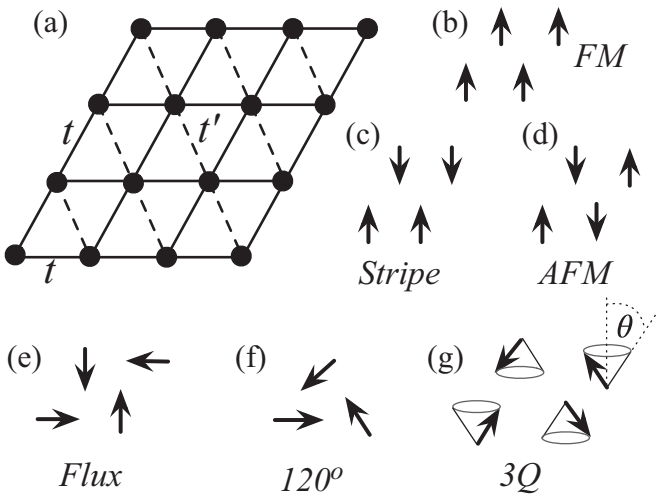

FIG. 1. (a) A schematic view of the anisotropic triangular lattice with hopping parameters t and t' shown via solid and dashed lines, respectively. (b)–(g) Building blocks of various long-range ordered magnetic phases. The cone angle θ connects the flux state to the antiferromagnetic state via the 3Q state.

density-versus-interaction phase diagram and then discuss the phase diagrams corresponding to specific electronic filling. In Sec. V we analyze the effect of nearest-neighbor Coulomb repulsion on the magnetic phase diagram. Conclusions are presented in Sec. VI.

II. MODEL

The single-orbital Hubbard Hamiltonian on an anisotropic triangular lattice is given by

$$H = -t(t')\sum_{\langle ij\rangle,\sigma} c^{\dagger}_{i\sigma}c_{j\sigma} - \mu\sum_{i} n_i + U\sum_{i} n_{i\uparrow}n_{i\downarrow}, \quad (1)$$

where $c^{\dagger}_{i\sigma}$ ($c_{i\sigma}$) is the creation (annihilation) operator, and $n_{i\sigma} = c^{\dagger}_{i\sigma}c_{i\sigma}$ is the number operator for electrons with spin $\sigma = \uparrow, \downarrow$ at site i. The total number operator for electrons at site i is $n_i = n_{i\uparrow} + n_{i\downarrow}$, and μ is the chemical potential. The electronic hopping amplitudes between nearest-neighbor sites on a triangular lattice are t and t' as shown in Fig. 1, and U denotes the on-site Hubbard repulsion.

The Hubbard model is one of the most successful and well studied Hamiltonians in condensed-matter physics [30]. However, due to its relevance to various materials, certain filling fractions have been of more interest than others. For instance, the model on a square lattice ($t' = 0$) has been studied in great detail near half filling. Very few studies have explored the possibility for noncollinear and noncoplanar phases [31,32]. The half-filled case on a triangular lattice has also been explored in search of spin-liquid phases, as the large-U limit of the Hubbard model leads to the spin-1/2 Heisenberg model which is frustrated on the triangular geometry. There have been studies for the quarter-filled case, which describes the physics of organic charge transfer salts [28,33,34]. The filling fraction of $n = 2/3$ has also been of interest due to its relevance to layered $AgNiO_2$ and $NaCoO_2$. A systematic search for noncollinear and, in particular, noncoplanar phases over the full range of electronic densities has not been reported even at the mean-field level.

III. VARIATIONAL MEAN-FIELD SCHEME

We determine the ground-state phase diagrams by performing a systematic search in the phase space of various ordered magnetic configurations. This is achieved by making use of the rotational invariance of the Hubbard Hamiltonian [35]. Before describing the details of the rotationally invariant scheme, let us recall the commonly used unrestricted Hartree-Fock (UHF) method. In this method, the interaction term is decoupled into charge and spin sectors. Ignoring the second-order term in fluctuations, the Hamiltonian reduces to the well-known form

$$\begin{aligned} H = &-t(t')\sum_{\langle ij\rangle\sigma} c^{\dagger}_{i\sigma}c_{j\sigma} - \mu\sum_{i} n_i \\ &+(1-\lambda)U\sum_{i}[\langle n_{i\downarrow}\rangle n_{i\uparrow} + \langle n_{i\uparrow}\rangle n_{i\downarrow} - \langle n_{i\downarrow}\rangle\langle n_{i\uparrow}\rangle] \\ &-\lambda U\sum_{i}[\langle s^{+}_i\rangle s^{-}_i + \langle s^{-}_i\rangle s^{+}_i - \langle s^{+}_i\rangle\langle s^{-}_i\rangle], \end{aligned} \quad (2)$$

where $s^{+}_i = c^{\dagger}_{i\uparrow}c_{i\downarrow}$ and $s^{-}_i = c^{\dagger}_{i\downarrow}c_{i\uparrow}$ are the spin operators. The variational parameter λ determines the relative contribution of the Hartree and the Fock terms in the mean-field decoupling.

In the UHF approach, the site dependence of the quantum averages is retained. Starting from a random guess for the various mean-field parameters, the Hamiltonian is diagonalized iteratively until self-consistency is achieved. In principal, the self-consistent solution depends on the starting configuration of mean-field parameters. Therefore, it is required to use a large number of starting configurations. The reliability of the final solution obtained in this way depends to a large extent on the complexity of the energy landscape. The ground-state degeneracies present in the case of frustrated lattices suggest that the converged solution could be a metastable state. In addition, λ should be determined via an energy minimization over the various self-consistent solutions. Although this scheme can capture the conventional ordered magnetic phases very well, it can easily miss unusual noncollinear and noncoplanar magnetic orderings.

Motivated by the appearance of such unusual magnetically ordered phases in a Kondo-lattice model, we search for similar magnetic phases in the Hubbard model. For this purpose, we recast the mean-field decouplings in a way that allows us to systematically search for a variety of ordered phases. We begin by rewriting the Hamiltonian in a reference frame with site-dependent spin-quantization axes [35]. This is done by performing a site-dependent SU(2) rotation of the quantization axes, given by

$$\begin{aligned} \begin{bmatrix} c_{i\uparrow} \\ c_{i\downarrow} \end{bmatrix} &= \begin{bmatrix} \cos\left(\frac{\theta_i}{2}\right)e^{i\frac{\phi_i}{2}} & -\sin\left(\frac{\theta_i}{2}\right)e^{i\frac{\phi_i}{2}} \\ \sin\left(\frac{\theta_i}{2}\right)e^{-i\frac{\phi_i}{2}} & \cos\left(\frac{\theta_i}{2}\right)e^{-i\frac{\phi_i}{2}} \end{bmatrix}\begin{bmatrix} d_{ip} \\ d_{ia} \end{bmatrix} \\ &\equiv \mathcal{R}(\theta_i,\phi_i)\begin{bmatrix} d_{ip} \\ d_{ia} \end{bmatrix}, \end{aligned} \quad (3)$$

where d_{ip} (d_{ia}) are annihilation operators for an electron at site i with spin parallel (antiparallel) to the quantization axis. A simple Hartree decoupling of the transformed Hamiltonian

leads to

$$H = -t(t')\sum_{\langle ij\rangle}\sum_{\sigma\sigma'}(f_{\sigma\sigma'}d^{\dagger}_{i\sigma}d_{j\sigma'} + \text{H.c.}) + U\sum_{i}[\langle n_{ip}\rangle n_{ia} + \langle n_{ia}\rangle n_{ip} - \langle n_{ip}\rangle\langle n_{ia}\rangle], \quad (4)$$

where $n_{i\sigma} = d^{\dagger}_{i\sigma}d_{i\sigma}$ and σ can take two values. The coefficients $f_{\sigma\sigma'}$ are explicitly given by

$$\begin{bmatrix} f_{pp} & f_{pa} \\ f_{ap} & f_{aa} \end{bmatrix} = \mathcal{R}^{\dagger}(\theta_i,\phi_i)\cdot\ \mathcal{R}(\theta_j,\phi_j). \quad (5)$$

We consider two broad categories of variational states. The first one is the set of general noncoplanar spiral states which can be parametrized by a cone angle Θ and a spiral wave vector $\mathbf{q}$ [36]. The polar and azimuthal angles of the spins are then given by $\theta_i = \Theta$ and $\phi_i = \mathbf{q}\cdot\mathbf{r}_i$.

The other set of states are the block-periodic states, where the spin configuration of an $m_x \times m_y$ block is repeated periodically to generate the configuration over the entire lattice. The choice of these variational states is motivated by the presence of various long-range ordered phases in the corresponding Kondo-lattice model. The flux state and the noncoplanar states shown in Fig. 1 are examples of the 2×2 block-periodic states. In the flux state the azimuthal angles change by $\pi/2$ as one goes from site 1 to site 4, while the polar angle remains equal to $\pi/2$. The noncoplanar state can be obtained from the flux state by changing the polar angles of the four spins as shown in Fig. 1. Similarly we take a 3×3 block to capture the 120° state, which can be connected to a ferromagnetic state by varying the polar angle from $\pi/2$ to 0. In order to allow for the six-sublattice noncollinear charge-ordered (NC-CO) state at $n = 2/3$, we take a 6×6 cluster as the building block [19]. The calculations have been performed in both canonical and grand-canonical approaches. In the grand-canonical (canonical) approach, we seek a self-consistent solution for a given fixed value of chemical potential (density) for all the variational states discussed above. In cases where more than one self-consistent solution exists, the lower-energy solution is selected and the corresponding state is taken as the mean-field ground state at that value of the chemical potential (density). For the grand-canonical approach, the density corresponding to the ground-state solution is calculated at the given value of the chemical potential and the phase diagrams are presented with density as a parameter.

IV. RESULTS AND DISCUSSIONS

In this section we present the results obtained by using the mean-field decoupling scheme described in the previous section. For most of the calculations we used $N = 64^2$ k-points in the first Brillouin zone. Results have also been checked for $N = 128^2$ in some cases. In the following section we discuss the n-U phase diagrams for different values of t'/t.

A. n-U phase diagrams

The n-U phase diagrams are obtained within the grand-canonical approach. The energy minimization over the two sets of variational states is performed for a fixed value of chemical potential μ. The chemical potential is then systematically varied in order to obtain different average electronic densities. The total energy is computed at zero temperature, where the Fermi function simply becomes a step function. The grand-canonical approach has an advantage in that it allows for the phase separation regions, which commonly arise in electronic systems, to be easily captured.

For $t'/t = 0$, the hopping connectivity is that of a square lattice. Therefore, in this case we display the density range $0 < n < 1$ in the phase diagram as the system is particle-hole symmetric [see Fig. 2(a)]. The square-lattice phase diagram is dominated by three simple phases: a Fermi liquid state for weak to intermediate U and away from $n = 1$, an antiferromagnetic (AFM) state near $n = 1$, and a ferromagnetic (FM) state for large U and away from $n = 1$. In addition, in the intermediate-U range we find a flux phase and a narrow window of phase separation close to $n = 1/2$. The flux phase is known to exist in the Kondo-lattice model with a classical approximation for local moments [18,37–39]. It has also been reported recently in the UHF study of a five-orbital Hubbard model for iron pnictides [40]. The planar spiral states are stable over a wide range of parameters. Next, we present the phase diagram for the anisotropic case where the particle-hole symmetry does not hold. Therefore, the density range displayed in Figs. 2(b)–2(d) is $0 < n < 2$. The FM state is strongly suppressed by the triangular anisotropy in the low-density regime, whereas it still dominates the large-density regime. This can be explained by invoking the Stoner picture for ferromagnetism: the triangular lattice density of states is higher if the Fermi level is located close to $n = 3/2$ and therefore the Stoner criterion for ferromagnetism can be satisfied for relatively small values of U. The flux state remains stable in a narrow window around intermediate U and $n = 1/2$. A new magnetically ordered state enters the phase diagram near $n = 1$. This is the well-known 120° state, which is the classical ground state of a triangular-lattice Heisenberg model. A wider window of phase separation appears in the $n > 1$ regime, where a conical spiral state also becomes stable. The phase diagram remains qualitatively similar between $t'/t = 0.5$ and $t'/t = 0.7$. However, the isotropic triangular case ($t' = t$) gives rise to new and interesting phases. The first of these new phases is the four-sublattice noncoplanar order near $n = 1/2$. This unusual magnetic state, also known as the 3Q state, is of wide interest as it supports a nonvanishing scalar spin chirality and an associated quantized Hall conductivity [12,14]. The quantized Hall conductivity is related to the nontrivial topology of the electronic band structure that the 3Q state induces in the Kondo Hamiltonians [41]. Interestingly, the 3Q state was predicted to be stable in the Hubbard model at $n = 3/2$ based on Fermi surface nesting arguments [12]. This has further been analyzed recently in the weak-coupling limit of the Hubbard model [42]. We find that the 3Q state is stable at $n = 3/2$ only for $U \leqslant 3$ and loses to FM order for larger values of U. This is in agreement with the weak-coupling analysis of the Hubbard model [42]. The second new state that appears exactly at $n = 2/3$ is the recently reported six-sublattice NC-CO state. In addition, the (π,π) ordered AFM state completely disappears, and instead the 120° state dominates the phase diagram near $n = 1$, as expected [43–46].

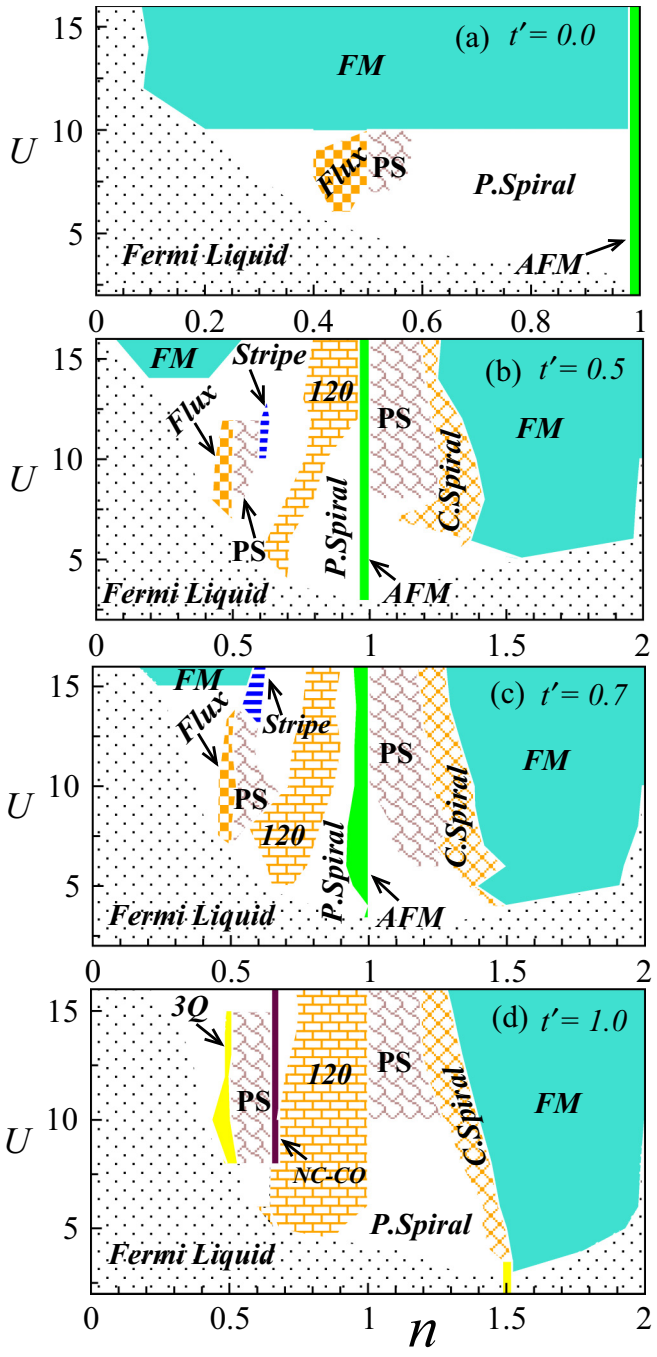

FIG. 2. n-U phase diagrams obtained within the grand-canonical approach for (a) $t'/t = 0$, (b) $t'/t = 0.5$, (c) $t'/t = 0.7$, and (d) $t'/t = 1$. PS denotes phase separation, P. spiral (C. spiral) refers to planar (conical) spiral phase, and 3Q and NC-CO are the four-sublattice and six-sublattice ordered phases found at $n = 1/2$ and $n = 2/3$, respectively.

Having discussed the overall structure of the n-U phase diagrams, we now examine more closely the effect of anisotropic hopping connectivity on different magnetic phases at specific filling fractions.

B. t'-U phase diagrams at $n = 1/2, 2/3, 1$, and $3/2$

In this section we describe the t'-U phase diagrams obtained within the canonical ensemble approach, where the minimization is performed over the variational parameters for a fixed value of the average electronic density n. We discuss the evolution of various phases as the lattice connectivity changes from square type to triangular type. The noncollinear flux phase is the lowest energy state for an unfrustrated square lattice ($t'/t = 0$) at $n = 1/2$ for intermediate coupling strength. This state remains stable in a wide parameter regime, $0 \leqslant t'/t \leqslant 0.8$. In fact, the stability window of the flux state widens in terms of the U values upon increasing t'/t [see Fig. 3(a)]. For $t'/t > 0.8$, a noncoplanar state becomes stable which evolves into the 3Q state at $t'/t = 1$. The evolution from the flux state to the 3Q noncoplanar state is depicted by the change in variational angle θ [see Fig. 4(a)]. For the flux state $\theta = \pi/2$, whereas for the perfect 3Q state $\theta \approx 0.98$. The other effect of the triangular geometry for $n = 1/2$ is to suppress the FM phase. The FM phase gives way to planar spiral phases even for small values of the parameter t'/t. The transition from a nonmagnetic Fermi liquid state to a magnetic state also occurs at a slightly larger value of U for the triangular lattice in comparison to the square lattice.

Another unusual six-sublattice magnetic order was recently reported in the Kondo-lattice model for an average density of two electrons per three sites [19]. In order to explore the possibility of this phase in the Hubbard model, we focus on the filling fraction of $n = 2/3$ [see Fig. 3(b)]. We again find that the FM state is suppressed in favor of the planar spiral states. Additionally the 120° order is stable for $t'/t > 0.5$. It is interesting to note that the stability window of the 120° state at $n = 2/3$ is even wider than that at $n = 1$. Importantly, we find that the six-sublattice NC-CO order is the ground state for $t'/t > 0.93$ and for $U > 7$.

The half filling, $n = 1$, is the most commonly studied filling fraction in the Hubbard models on triangular and square lattices [47]. Within the mean field, we find that the AFM order is robust and is stable in the regime $0 < t'/t < 0.7$. Beyond $t'/t = 0.7$, the AFM order continuously evolves towards the 120° state. In Fig. 4(a), we show the change in the spiral wave vector (q_x, q_y) from (π,π) to $(2\pi/3, 2\pi/3)$. The half-filling case is also of interest for the possible existence of a spin-liquid state [48]. However, our mean-field method does not capture the spin-liquid states and therefore we cannot comment on this competition in the present paper. Some earlier studies that capture the electronic correlations beyond the mean-field level show that a nonmagnetic insulating phase can exist between the antiferromagnetic insulator and the paramagnetic metal phase [49,50].

Finally we discuss the filling fraction $n = 3/2$, which is interesting due to the presence of the Fermi-surface nesting feature in the noninteracting Hamiltonian. In fact, the noncoplanar 3Q state was first predicted based on the nesting property of the Fermi surface. Clearly, for small U the 3Q state is the ground state due to the presence of a peculiar Fermi surface nesting in the noninteracting Hamiltonian [12]. Interestingly, the 3Q order loses to FM order for $U > 3$. The relative stability of the 3Q state at $n = 1/2$ and $n = 3/2$

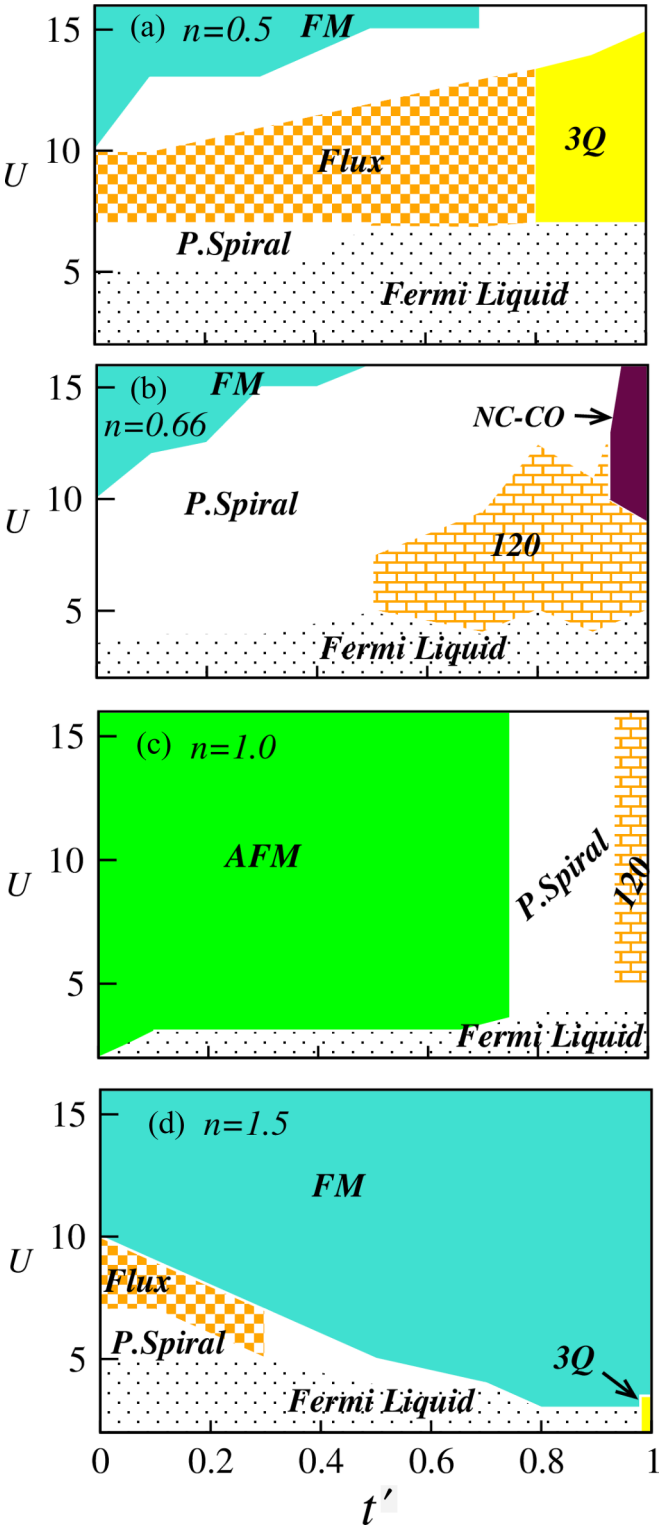

FIG. 3. t'-U phase diagrams obtained within the canonical ensemble approach at commensurate values of average electronic fillings: (a) $n = 1/2$, (b) $n = 2/3$, (c) $n = 1$, and (d) $n = 3/2$. The notation for different phases is same as that in Fig. 2.

was also explored in the Kondo-lattice Hamiltonian with a conclusion that the window of stability of the 3Q state is wider for $n = 1/2$ compared to $n = 3/2$ [14]. Our calculations on the Hubbard model support the results of the corresponding

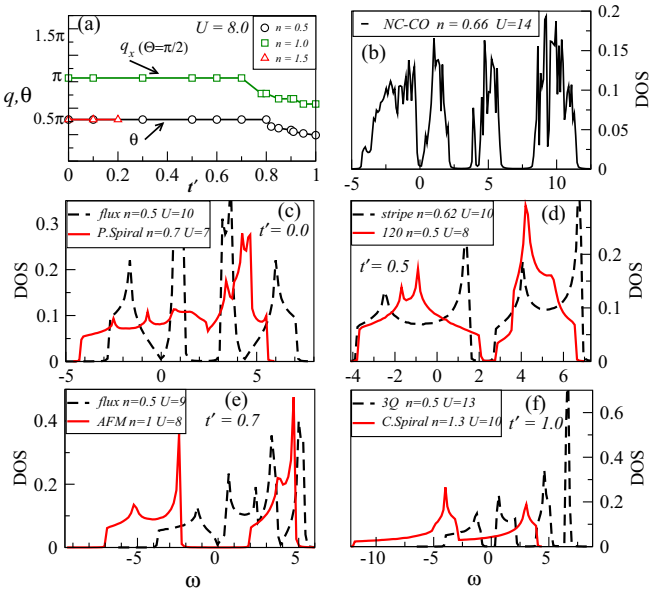

FIG. 4. (a) Change in the variational parameters corresponding to the ground states for $n = 1/2$, $n = 1$, and $n = 3/2$ as a function of t'. The parameters are the spiral wave vector $q_x = q_y$ for $n = 1$, and the polar angle θ describing the 2×2 block-periodic states for $n = 1/2,3/2$. For $n = 3/2$ the ground state is FM for $t'/t > 0.2$. The electronic density of states for various ground states for different values of t' are as follows: (b) the NC-CO state at $n = 2/3$ and $t' = 1$; (c) the flux and planar spiral states at $n = 0.5$ and $n = 0.7$, respectively, for $t' = 0$; (d) the stripe and 120° states at $n = 0.62$ and $n = 0.5$, respectively, for $t'/t = 0.5$; (e) the flux and the staggered AFM states for $t'/t = 0.7$; and (f) the noncoplanar 3Q and conical spiral states for $t'/t = 1$.

Kondo-lattice model. In sharp contrast to the quarter filling ($n = 1/2$), the three-quarter filling favors a FM state for increasing t'/t. As mentioned earlier, this can be understood from the particle-hole asymmetry and large density of states (DOS) in the $n > 1$ regime for the triangular lattice.

The electronic spectrum corresponding to different phases is displayed in the plots for the density of states in Figs. 4(b)–4(f). The DOS is defined as

$$D(\omega) = \frac{1}{N}\sum_k \delta(\omega - \epsilon_k) \approx \frac{1}{N}\sum_k \frac{\gamma/\pi}{[\gamma^2 + (\omega - \epsilon_k)^2]}, \quad (6)$$

where ϵ_k are the eigenvalues corresponding to the lowest-energy self-consistent solution, δ is the Dirac delta function, and γ is the broadening parameter which we take to be $0.02t$ for calculations. All three possible varieties of the spectra are present: The spiral states are metallic, the 3Q is noncoplanar, the (π,π) AFM and the NC-CO states are insulating, and the flux state is semimetallic with a graphenelike DOS. A robust gap in the DOS is suggestive of the stability of these phases against higher-order quantum corrections.

V. EFFECT OF INTERSITE COULOMB REPULSION ON MAGNETICALLY ORDERED PHASES

In this section we analyze the influence of nearest-neighbor (NN) Coulomb repulsion on various magnetic phases

discussed so far. We begin by extending the Hubbard model, Eq. (1), by including a NN repulsion. The extended Hubbard Hamiltonian is given by

$$H' = H + V(V') \sum_{\langle ij \rangle} n_i n_j. \tag{7}$$

The parameters V and V' denote the strength of the Coulomb repulsion along inequivalent directions on the anisotropic triangular lattice. It is well known that NN Coulomb repulsion in bipartite lattices favors charge ordering [33]. However, the triangular geometry frustrates the checkerboard-type charge ordering and leads to exotic charge-ordered phases, such as the pinball liquid and inverse pinball liquid [51–54].

The parameter space for the Hamiltonian Eq. (7) comprises t', U, V, V', and n as independent parameters. Clearly, a complete exploration of this large parameter space for various spin- and charge-ordered phases is easily a topic of an independent study. Here, our primary focus is to test the stability against the intersite Coulomb repulsion of the ordered magnetic phases obtained in the Hubbard model. The effect of the NN Coulomb repulsion is to promote charge ordering. The system can either acquire a pure charge-ordered state with no magnetic moments, or the charge order can be accommodated within the magnetically ordered state. Given that the focus of the present paper is on unconventional magnetic order, we focus on the latter scenario. Therefore, we describe the fate of each of the unconventional magnetically ordered states in the presence of the NN Coulomb interactions.

The flux state at $n = 1/2$. We present results for the quarter-filled case where the interesting mean-field ground states are the flux state, for $t'/t \leqslant 0.8$, and noncoplanar states for $t'/t > 0.8$. We use the variational scheme corresponding to the block-periodic states discussed in Sec. III. This allows for four inequivalent sites in terms of the spin and charge structures. The planar structure is fixed to be of the flux type and the polar angle is varied to obtain magnetic phases that interpolate between the flux and the (π,π) AFM state via the 3Q state (see Fig. 1). Results for $V' = 0$ are summarized in Fig. 5. We find that the flux state ($t'/t = 0$) is compatible with stripe charge ordering. Indeed, the charge disproportionation $n_B - n_A$ becomes finite as soon as $V \neq 0$ [see Fig. 5(a)]. The magnetic structure retains the flux character; however, the magnetic moments become unequal on sites A and B [see Figs. 6(a)–6(c)]. For very large values of V the magnetic moment becomes vanishingly small at one of the sites, leading to a strongly charge-ordered AFM state. In fact, a similar state has been reported in the quarter-filled Hubbard-Holstein and Kondo-lattice models on a square lattice [55,56]. The nature of the magnetic order is depicted by the value of the variational polar angle θ corresponding to the minimum-energy self-consistent solution. $\theta = \pi/2$ remains constant for $t'/t = 0$ [see inset in Fig. 5(d)].

The 3Q state at $n = 1/2$. In contrast to the flux state, the 3Q state competes with charge ordering. It is easy to understand this difference from the energetics: charge ordering leads to lowering of energy via opening an energy gap in the spectrum. Since the flux state is gapless, a gap opening lowers the energy and therefore the ground state develops a charge ordering even

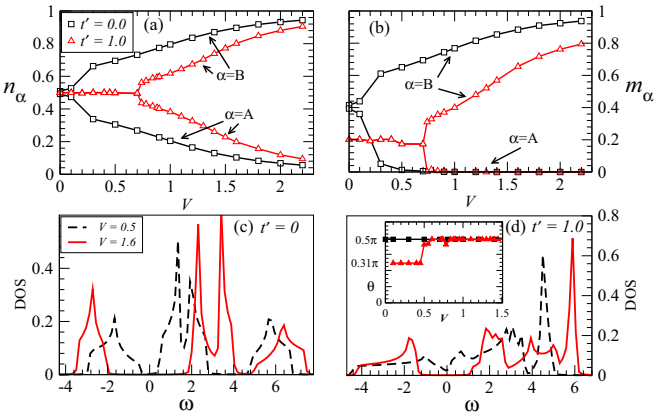

FIG. 5. Results on the effect of Coulomb repulsion at $n = 1/2$. The value of (a) the local charge densities and (b) the local magnetic moments at two inequivalent sites as a function of V. The inset in (d) shows the change in variational angle θ which connects the flux state ($\theta = \pi/2$) to the 3Q state ($\theta \sim 0.31\pi$). Density of states of the spin-charge ordered phases at different values of V for (c) $t' = 0$ and (d) $t' = 1$. These results are obtained for $U = 8$ and $V' = 0$.

for small values of V. However, the 3Q state is already gapped with the origin of the gap tied to peculiar magnetic structure. Therefore, in order to further lower the energy the charge ordering must open a gap that offsets the 3Q gap. Starting with $t'/t = 1$, the charge disproportionation remains zero until $V = 0.7$. A weak reduction of the magnetic moment occurs near $V = 0.5$ together with a deviation from the ideal 3Q structure. Near $t'/t = 0.7$, $n_B - n_A$ becomes finite, and the magnetic

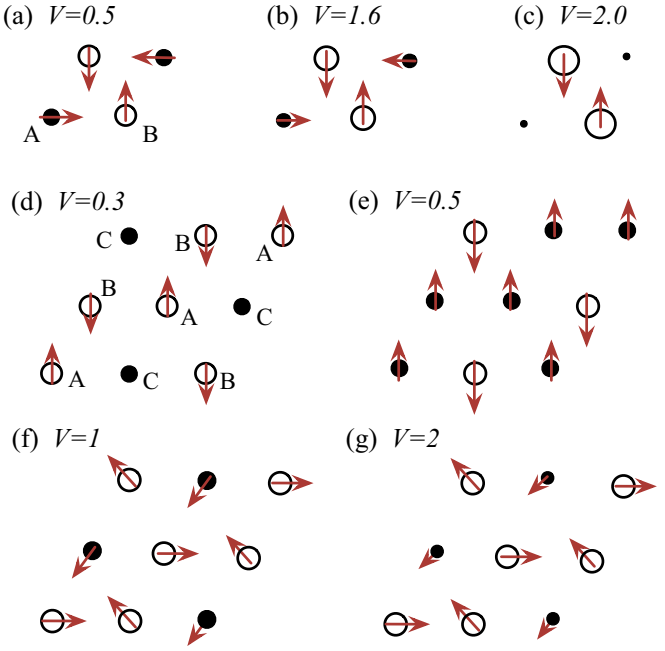

FIG. 6. A schematic view of the spin-charge ordered phases that appear for finite intersite Coulomb interaction for filling fraction: (a)–(c) $n = 1/2$, $t' = 0$ and (d)–(g) $n = 2/3$, $t' = t$. The sizes of the circles represent the local charge density. The higher-density sites are shown as open circles for clarity.

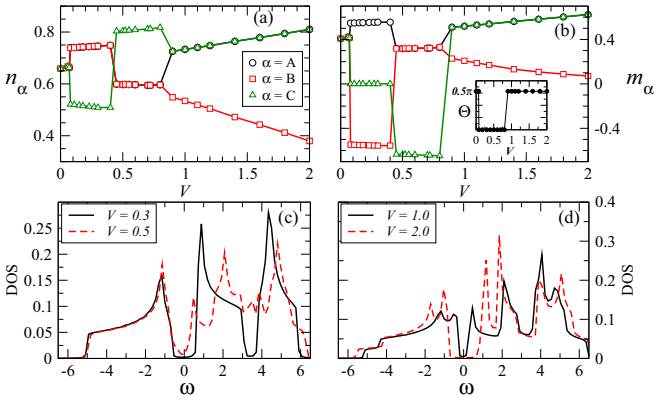

FIG. 7. Results on the effect of Coulomb repulsion at $n = 2/3$. The value of (a) the local charge densities and (b) the local magnetic moments of three inequivalent sites as a function of V for $V' = 0$. The inset in (b) shows the change in variational angle Θ which connects the FM state ($\Theta = 0$) to the 120° state ($\Theta = \pi/2$). (c)-(d) Density of states of the spin-charge ordered phases at different values of V. These results are obtained for $U = 8$ and $V' = 0$.

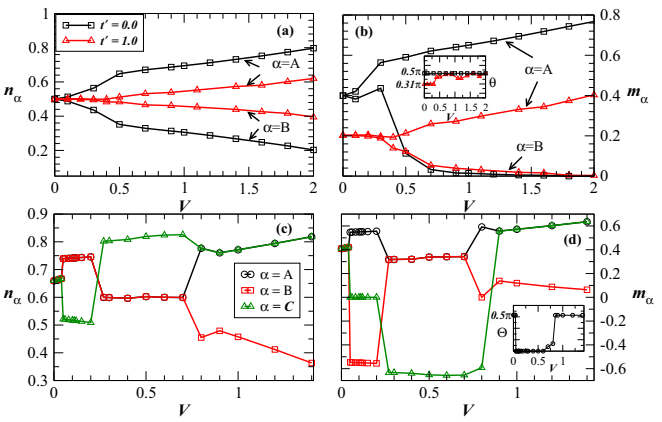

FIG. 8. The value of (a) the local charge densities and (b) the local magnetic moments at two inequivalent sites as a function of V for $n = 1/2$. The value of (c) the local charge densities and (d) the local magnetic moments at three inequivalent sites as a function of V for $n = 2/3$. These results are obtained for $U = 8$ and $V' = V$.

moment at site A vanishes, leading to the same charge-ordered AFM state as for $t' = 0$. Therefore, in this case the 3Q state is destabilized at the onset of charge ordering. The density of states [Figs. 5(c) and 5(d)] show that a gap opens in the electronic spectrum owing to the charge ordering. Thus, the semimetallic flux state is turned into a fully gapped flux state, and eventually into a gapped collinear AFM for large V.

The 120° state at $n = 2/3$. Finally, we study the effect of Coulomb repulsion on the 120° phase. The results are presented in Fig. 7. The 120° state is destabilized in favor of a collinear state containing three inequivalent sites. Two of the sites have equal charge density which is larger than that on the third ($n_A = n_B > n_C$). The magnetic moments on the low-charge sites vanish, while those on the other two sites are antialigned [see Figs. 7(a), 7(b) and Fig. 6(d)]. The resulting spin-charge order can be visualized as two interpenetrating lattices: an AFM ordered honeycomb lattice and a nonmagnetic triangular lattice. This spontaneous separation into two sublattices is similar to what happens in the pinball-liquid phase, the crucial difference being the insulating character of the DOS in the present case. For $V > 0.4$, the charge densities on the three sites are given by $n_A = n_B < n_C$, and all three sites have finite magnetic moments. The resulting state with up-up-down structure has also been found as the ground state of the Ising spin Kondo-lattice model. For $V \geqslant 0.9$ the charge densities at three sites are given by $n_A = n_C > n_B$, and the magnetic state again becomes noncollinear [see inset in Fig. 7(b)]. Upon a further increase of V the charge density as well as the magnetic moment on one of the sites keeps reducing, giving rise to an effective honeycomb lattice for the electrons.

For the flux state, the 3Q state, and the 120° state at $n = 2/3$, the results for $V' = V$ are qualitatively similar to those for $V' = 0$. We show this explicitly in Fig. 8 by plotting the values of the local charge densities and the local magnetic moments for inequivalent sites in different spin-charge ordered states. For the flux state, the charge inequivalence between two sites is induced for any finite value of $V = V'$, and for the 3Q state a critical value of V is required in order for the charge inequivalence to appear. This is similar to the case of $V' = 0$ [compare Figs. 8(a) and 8(b) with Figs. 5(a) and 5(b)]. Similarly, for the 120° state at $n = 2/3$ the sequence in which the three sites become charge and spin inequivalent for $V = V'$ is identical to that for $V' = 0$ [compare Figs. 8(c) and 8(d) with Figs. 7(a) and 7(b)]. Therefore, the results for the above magnetically ordered phases are qualitatively similar for the cases $V' = 0$ and $V' = V$. The key difference is a reduced value of charge disproportionation in the case of $V' = V$ compared to that in $V' = 0$.

Other than the three phases discussed above, all other magnetically ordered phases become unstable towards pure charge-ordered states for finite V/V'. Given that the charge-ordered states can themselves appear in various varieties, including long-period modulations [57], it is a challenging task to explore the full parameter space of t', U, V, V', and n for all possible spin- and charge-ordered phases. This can be taken up as an independent study in the future.

VI. CONCLUSIONS

Motivated by the importance of noncollinear and noncoplanar magnetism in determining electronic properties, such as the anomalous Hall response, improper ferroelectricity, etc., a systematic search is carried out for unconventional magnetic ground states in the Hubbard model. Using a mean-field decoupling scheme that treats collinear, noncollinear, and noncoplanar order on equal footing, we uncover a rich magnetic phase diagram for the Hubbard Hamiltonian on an anisotropic triangular lattice. The most notable of the unconventional magnetic ground states are (i) the four-sublattice flux order, (ii) the 3Q noncoplanar state, and (iii) the six-sublattice noncollinear charge-ordered state. These states have been found as ground states of the Kondo-lattice model on a triangular lattice in previous studies [12–14,19]. The effect of nearest-neighbor Coulomb interactions on these magnetic states is also investigated and leads to some fascinating spin-

charge ordered phases. The flux state is found to be compatible with a stripelike charge-ordered arrangement, whereas the noncoplanar 3Q state competes with charge ordering and becomes unstable upon increasing the Coulomb interaction strength beyond a critical value. The spin-charge ordered state found at $n = 1/2$ is a triangular lattice version of the state found in quarter-filled Hubbard-Holstein and Kondo-lattice models [55,56]. The 120° state gives way to a sequence of spin-charge ordered states which lead to spontaneous decoupling of the triangular lattice into a honeycomb lattice and a triangular lattice. For a certain range of parameter values, one of the sublattices is magnetic while the other is nonmagnetic. This highly resembles the pinball-liquid state reported in theoretical studies of a multiband extended Hubbard model on a triangular lattice [58]. The phase diagrams presented here set the stage for further studies to analyze the stability of these phases. A number of states reported here possess a robust gap in the electronic spectrum and, therefore, are likely to remain stable against higher-order quantum effects. Given the fundamental nature of the Hubbard model, our study is of fundamental importance. In particular, the results are of relevance to various triangular lattice systems, such as the layered $AgNiO_2$ [21,22], the $NaCoO_2$ [23–27], and the organic crystals [28,29]. Many of the phases presented in this work are similar to the spin-charge ordered phases reported experimentally in these materials. While material-specific models have been proposed to understand these phases, it is interesting to see that the most elementary model for magnetism—the single-band Hubbard model—supports many of the unconventional spin-charge ordered states.

ACKNOWLEDGMENTS

The calculations were performed using the High Performance Computing Facility at IISER Mohali. K.P. acknowledges support via a CSIR/UGC fellowship. S.K. acknowledges support from the Department of Science and Technology (DST), India.

[1] C. Zener, Phys. Rev. **82**, 403 (1951).
[2] S. Maekawa, T. Tohyama, S. E. Barnes, S. Ishihara, W. Koshibae, and G. Khaliullin, *Physics of Transition Metal Oxides* (Springer Science & Business Media, New York, 2004), p. 340.
[3] J. Hubbard, Proc. R. Soc. London Ser. A **276**, 238 (1963).
[4] G. Stewart, Rev. Mod. Phys. **56**, 755 (1984).
[5] A. Auerbach, *Interacting Electrons and Quantum Magnetism* (Springer Science & Business Media, New York, 2012), p. 255.
[6] J. E. Hirsch, Phys. Rev. B **31**, 4403 (1985).
[7] N. Nagaosa, J. Sinova, S. Onoda, A. H. MacDonald, and N. P. Ong, Rev. Mod. Phys. **82**, 1539 (2010).
[8] I. Kézsmárki, S. Onoda, Y. Taguchi, T. Ogasawara, M. Matsubara, S. Iguchi, N. Hanasaki, N. Nagaosa, and Y. Tokura, Phys. Rev. B **72**, 094427 (2005).
[9] S. Hayami and Y. Motome, Phys. Rev. B **91**, 075104 (2015).
[10] H. Katsura, N. Nagaosa, and A. V. Balatsky, Phys. Rev. Lett. **95**, 057205 (2005).
[11] M. Mostovoy, Phys. Rev. Lett. **96**, 067601 (2006).
[12] I. Martin and C. D. Batista, Phys. Rev. Lett. **101**, 156402 (2008).
[13] S. Kumar and J. van den Brink, Phys. Rev. Lett. **105**, 216405 (2010).
[14] Y. Akagi and Y. Motome, J. Phys. Soc. Jpn. **79**, 083711 (2010).
[15] Y. Akagi, M. Udagawa, and Y. Motome, Phys. Rev. Lett. **108**, 096401 (2012).
[16] H. Ishizuka and Y. Motome, Phys. Rev. Lett. **109**, 237207 (2012).
[17] H. Ishizuka and Y. Motome, Phys. Rev. Lett. **108**, 257205 (2012).
[18] J. W. F. Venderbos, M. Daghofer, J. van den Brink, and S. Kumar, Phys. Rev. Lett. **109**, 166405 (2012).
[19] S. Reja, R. Ray, J. van den Brink, and S. Kumar, Phys. Rev. B **91**, 140403 (2015).
[20] G.-W. Chern, Phys. Rev. Lett. **105**, 226403 (2010).
[21] E. Wawrzyńska, R. Coldea, E. M. Wheeler, T. Sörgel, M. Jansen, R. M. Ibberson, P. G. Radaelli, and M. Koza, Phys. Rev. B **77**, 094439 (2008).
[22] E. Wawrzyńska, R. Coldea, E. M. Wheeler, I. I. Mazin, M. D. Johannes, T. Sörgel, M. Jansen, R. M. Ibberson, and P. G. Radaelli, Phys. Rev. Lett. **99**, 157204 (2007).
[23] I. R. Mukhamedshin, I. F. Gilmutdinov, M. A. Salosin, and H. Alloul, JETP Lett. **99**, 471 (2014).
[24] I. Mukhamedshin and H. Alloul, Physica B: Condens. Matter **460**, 58 (2014).
[25] I. R. Mukhamedshin, H. Alloul, G. Collin, and N. Blanchard, Phys. Rev. Lett. **93**, 167601 (2004).
[26] C. Bernhard, A. V. Boris, N. N. Kovaleva, G. Khaliullin, A. V. Pimenov, L. Yu, D. P. Chen, C. T. Lin, and B. Keimer, Phys. Rev. Lett. **93**, 167003 (2004).
[27] H. Alloul, I. R. Mukhamedshin, T. A. Platova, and A. V. Dooglav, Europhys. Lett. **85**, 47006 (2009).
[28] C. Hotta, Crystals **2**, 1155 (2012).
[29] F. Kagawa, T. Sato, K. Miyagawa, K. Kanoda, Y. Tokura, K. Kobayashi, R. Kumai, and Y. Murakami, Nat. Phys. **9**, 419 (2013).
[30] J. P. F. LeBlanc, A. E. Antipov, F. Becca, I. W. Bulik, G. K.-L. Chan, C.-M. Chung, Y. Deng, M. Ferrero, T. M. Henderson, C. A. Jiménez-Hoyos, E. Kozik, X.-W. Liu, A. J. Millis, N. V. Prokof'ev, M. Qin, G. E. Scuseria, H. Shi, B. V. Svistunov, L. F. Tocchio, I. S. Tupitsyn, S. R. White, S. Zhang, B.-X. Zheng, Z. Zhu, and E. Gull (Simons Collaboration on the Many-Electron Problem), Phys. Rev. X **5**, 041041 (2015).
[31] A. Chubukov and K. Musaelian, Phys. Rev. B **51**, 12605 (1995).
[32] M. A. Ojeda, J. Dorantes-Dávila, and G. M. Pastor, Phys. Rev. B **60**, 6121 (1999).
[33] A. Amaricci, A. Camjayi, K. Haule, G. Kotliar, D. Tanasković, and V. Dobrosavljević, Phys. Rev. B **82**, 155102 (2010).
[34] L. F. Tocchio, C. Gros, X.-F. Zhang, and S. Eggert, Phys. Rev. Lett. **113**, 246405 (2014).
[35] H. J. Schulz, Phys. Rev. Lett. **65**, 2462 (1990).
[36] S. Kumar, J. van den Brink, and A. P. Kampf, Phys. Rev. Lett. **104**, 017201 (2010).
[37] D. F. Agterberg and S. Yunoki, Phys. Rev. B **62**, 13816 (2000).
[38] M. Daghofer, W. Koller, W. von der Linden, and H. Evertz, Physica B (Amsterdam, Neth.) **359–361**, 804 (2005).
[39] X. Chen, S. Dong, and J.-M. Liu, Phys. Rev. B **81**, 064420 (2010).

[40] Q. Luo and E. Dagotto, Phys. Rev. B **89**, 045115 (2014).
[41] S. Kourtis, J. W. F. Venderbos, and M. Daghofer, Phys. Rev. B **86**, 235118 (2012).
[42] G.-W. Chern and C. D. Batista, Phys. Rev. Lett. **109**, 156801 (2012).
[43] H. R. Krishnamurthy, C. Jayaprakash, S. Sarker, and W. Wenzel, Phys. Rev. Lett. **64**, 950 (1990).
[44] C. Jayaprakash, H. R. Krishnamurthy, S. Sarker, and W. Wenzel, Europhys. Lett. **15**, 625 (1991).
[45] K. Machida and M. Fujita, Phys. Rev. B **42**, 2673(R) (1990).
[46] M. Fujita, T. Nakanishi, and K. Machida, Phys. Rev. B **45**, 2190 (1992).
[47] M. Laubach, R. Thomale, C. Platt, W. Hanke, and G. Li, Phys. Rev. B **91**, 245125 (2015).
[48] L. F. Tocchio, H. Feldner, F. Becca, R. Valentí, and C. Gros, Phys. Rev. B **87**, 035143 (2013).
[49] H. Morita, S. Watanabe, and M. Imada, J. Phys. Soc. Jpn. **71**, 2109 (2002).
[50] T. Mizusaki and M. Imada, Phys. Rev. B **74**, 014421 (2006).
[51] M. Miyazaki, C. Hotta, S. Miyahara, K. Matsuda, and N. Furukawa, J. Phys. Soc. Jpn. **78**, 014707 (2009).
[52] J. Merino, A. Ralko, and S. Fratini, Phys. Rev. Lett. **111**, 126403 (2013).
[53] T. Watanabe, H. Yokoyama, Y. Tanaka, and J. Inoue, Phys. Rev. B **77**, 214505 (2008).
[54] H. Watanabe and M. Ogata, J. Phys. Soc. Jpn. **74**, 2901 (2005).
[55] S. Kumar and J. van den Brink, Phys. Rev. B **78**, 155123 (2008).
[56] T. Misawa, J. Yoshitake, and Y. Motome, Phys. Rev. Lett. **110**, 246401 (2013).
[57] M. Naka and H. Seo, J. Phys. Soc. Jpn. **83**, 053706 (2014).
[58] A. Ralko, J. Merino, and S. Fratini, Phys. Rev. B **91**, 165139 (2015).